



**Investigation of Ternary Metal Dodecaborides ( $M_1M_2M_3$ )B<sub>12</sub>  
( $M_1$ ,  $M_2$  and  $M_3$  = Zr, Y, Hf and Gd)**

Journal:	<i>Dalton Transactions</i>
Manuscript ID	DT-ART-02-2018-000563.R1
Article Type:	Paper
Date Submitted by the Author:	26-Mar-2018
Complete List of Authors:	Akopov, Georgiy; University of California Los Angeles, Chemistry and Biochemistry Roh, Inwhan; University of California Los Angeles, Chemistry and Biochemistry Sobell, Zachary; University of Colorado Boulder, Chemistry Yeung, Michael; Northwestern University, Chemistry Kaner, Richard; University of California Los Angeles, Chemistry and Biochemistry

**Investigation of Ternary Metal Dodecaborides ( $M_1M_2M_3$ )B<sub>12</sub> ( $M_1$ ,  $M_2$  and  $M_3$  = Zr, Y, Hf and Gd)**

*Georgiy Akopov<sup>1</sup>, Inwhan Roh<sup>1</sup>, Zachary C. Sobell<sup>1</sup>, Michael T. Yeung<sup>2</sup>, and Richard B. Kaner<sup>1,3,4\*</sup>*

<sup>1</sup>*Department of Chemistry and Biochemistry, University of California, Los Angeles (UCLA), Los Angeles, CA 90095, USA*

<sup>2</sup>*Department of Chemistry, Northwestern University, Evanston, IL 60208, USA*

<sup>3</sup>*Department of Materials Science and Engineering, University of California, Los Angeles (UCLA), Los Angeles, CA 90095, USA*

<sup>4</sup>*California NanoSystems Institute (CNSI), University of California, Los Angeles (UCLA), Los Angeles, CA 90095, USA*

\* Corresponding author: kaner@chem.ucla.edu

## ABSTRACT

Samples of metal borides with a nominal composition of  $((M_1)_{(1-x-z)}(M_2)_{(x)}(M_3)_{(z)}) : 20B$  ( $M_1$ ,  $M_2$  and  $M_3 = \text{Zr, Y, Hf and Gd}$ ) were prepared by arc-melting and studied for phase composition (using powder X-ray diffraction (PXRD) and energy dispersive X-ray spectroscopy (EDS)) and mechanical properties (Vickers hardness). Ternary metal dodecaborides phases were successfully synthesized for the majority of compositions, including stabilization of two high-pressure (6.5 GPa) phases (cubic- $UB_{12}$  structure),  $\text{HfB}_{12}$  and  $\text{GdB}_{12}$ , in  $(\text{Zr}_{1-x-z}\text{Hf}_x\text{Gd}_z) : 20B$  and  $(\text{Y}_{1-x-z}\text{Hf}_x\text{Gd}_z) : 20B$  nominal alloy compositions. Unit cell refinement for the samples showed solid solution formation in most cases. Vickers hardness measurements indicated that most samples possess enhanced hardness in comparison to their parent phases, with the alloy  $(\text{Zr}_{0.50}\text{Y}_{0.25}\text{Gd}_{0.25}) : 20B$  having a hardness of  $46.9 \pm 2.4$  GPa compared to  $41.3 \pm 1.1$  and  $41.6 \pm 1.3$  GPa for alloy compositions of 1.0 Zr : 20B and 1.0 Y : 20B, respectively, at 0.49 N of applied load. Using the data from this manuscript as well as previous work, pseudo-ternary phase diagrams (at a constant boron content) have been constructed.

## INTRODUCTION

Metal borides possess a host of remarkable thermal<sup>1,2</sup>, optical, electronic and magnetic<sup>1,3,4</sup> properties. In addition, metal borohydrides and borates are good candidates for energy storage applications, through hydrogen storage.<sup>5,6</sup> This wide range of attributes is matched by a comparable variety of boride structures<sup>1,2,7-11</sup>: from sub-borides ( $M_4B$ )<sup>12</sup> and tetraborides ( $MB_4$ )<sup>13-15</sup> to dodecaborides ( $MB_{12}$ )<sup>16-19</sup> and even higher borides ( $MB_{50}$  and  $MB_{66}$ )<sup>20,21</sup>. Owing to boron's propensity to catenate, the higher borides possess extended boron networks, which results in prodigious mechanical properties.<sup>22</sup>

Amongst these higher borides, metal dodecaborides<sup>16</sup> ( $MB_{12}$ ) comprise a remarkable class of isotropic compounds, with interesting properties, such as superconductivity<sup>23</sup> and superhardness<sup>17,24</sup>. Metal dodecaborides crystallize in two structures which differ solely by the arrangement of their boron cuboctahedra: cubic- $UB_{12}$  ( $Fm\bar{3}m$ ) and tetragonal- $ScB_{12}$  ( $I4/mmm$ ) (**Figure 1**). For the cubic structure, the 24 boron atom cuboctahedron cages surrounding each 12 coordinate metal atom are arranged in a face-centered cubic (FCC) lattice, while the tetragonal structure has a body-centered tetragonal (BCT) arrangement. The main criterion for the formation of metal dodecaborides of the cubic- $UB_{12}$  structure under ambient pressure is the size of the metal, or more precisely, its radius in a 12 coordinate environment, with the smallest metal being zirconium (1.603 Å<sup>25</sup>) and largest yttrium (1.801 Å<sup>25</sup>). The metals are considered 12-coordinate since 12 boron-boron bonds are equidistant from each metal atom in the 24 boron atom cuboctahedron cage. These 12 coordinate metal radii have been calculated from close-packed elemental structures by using half of the interatomic distance.<sup>25-27</sup> When the size of the metal deviates from the 1.603-1.801 Å range even by a very small margin, like in the case of hafnium (1.580 Å<sup>25</sup>), the  $MB_{12}$  phase becomes unstable. However, it can be synthesized either

under high pressure (6.5 GPa)<sup>25</sup> or stabilized in an alloy with a stable dodecaboride ( $Y_{1-x}Hf_xB_{12}$ )<sup>19</sup>. The same is true for metals larger than yttrium (e.g. Gd, Sm, Nd, Pr and Th), they can either be synthesized under high pressure (e.g.  $ThB_{12}$  and  $GdB_{12}$ )<sup>28</sup> or stabilized in a matrix with a stable dodecaboride ( $Zr_{1-x}Th_xB_{12}$ <sup>23</sup>,  $Zr_{1-x}Gd_xB_{12}$ ,  $Zr_{1-x}Sm_xB_{12}$ ,  $Zr_{1-x}Nd_xB_{12}$  and  $Zr_{1-x}Pr_xB_{12}$ <sup>18</sup>).

In both cases, the ambient pressure stabilization worked based on the following principle: a “smaller atom dodecaboride” being stabilized in a framework formed by a “larger atom dodecaboride” ( $Y_{1-x}Hf_xB_{12}$ ) and vice versa ( $Zr_{1-x}Gd_xB_{12}$ ) so that the final composition’s lattice parameters fit within the region of dodecaboride formation. Stabilization and synthesis of high pressure phases under ambient pressure gives an easy avenue to study their properties. As the lattice parameters of high pressure  $HfB_{12}$  are too large (and likewise for high pressure  $GdB_{12}$  too small), it is interesting to study whether these high-pressure phases can stabilize each other under ambient pressure as well as their behavior in ternary metal dodecaboride systems. Furthermore, the stabilization of  $HfB_{12}$  and  $GdB_{12}$  in the same compound has the additional advantage of solid solution strengthening, where dislocation propagation is pinned by localized strain. This is a technique that had been tried with other dodecaborides.<sup>18,23,29</sup> The greater size difference between Gd and Hf should create the aforementioned micro-strain, which could significantly improve the mechanical properties and hardness.

In this manuscript we have synthesized four ternary boride systems with the following nominal compositions: ( $Zr_{1-x-z}Hf_xGd_z$ ) : 20B, ( $Y_{1-x-z}Hf_xGd_z$ ) : 20B, ( $Zr_{1-x-z}Hf_xY_z$ ) : 20B, ( $Zr_{1-x-z}Y_xGd_z$ ) : 20B and studied their phase composition and mechanical properties. We discovered that a ternary metal dodecaboride phase forms in most cases. Remarkably, it is possible to stabilize both high pressure phases ( $HfB_{12}$  and  $GdB_{12}$ ) in the matrixes of  $Zr_{1-x-z}Hf_xGd_zB_{12}$  and  $Y_{1-x-z}Hf_xGd_zB_{12}$ . A remarkable hardness increase of greater than 10% is observed in the alloy

( $\text{Zr}_{0.50}\text{Y}_{0.25}\text{Gd}_{0.25}$ ): 20B when compared to its parent compounds.

## EXPERIMENTAL PROCEDURE

Pellets of the following nominal compositions: ( $\text{Zr}_{1-x-z}\text{Hf}_x\text{Gd}_z$ ): 20B, ( $\text{Y}_{1-x-z}\text{Hf}_x\text{Gd}_z$ ): 20B, ( $\text{Zr}_{1-x-z}\text{Hf}_x\text{Y}_z$ ): 20B, ( $\text{Zr}_{1-x-z}\text{Y}_x\text{Gd}_z$ ): 20B ( $x$  and  $z = 0.25, 0.33$  and  $0.5$ ), ( $\text{Hf}_{1-x}\text{Gd}_x$ ): 20B, ( $x = 0.05, 0.25, 0.50, 0.75$  and  $0.95$ ), and ( $\text{Y}_{1-x}\text{Gd}_x$ ): 20B ( $x = 0.05, 0.25, 0.50, 0.70, 0.75$  and  $0.95$ ), were prepared from high-purity metal and boron powders: amorphous boron (99+%, Strem Chemicals, USA), gadolinium (99%, Sigma-Aldrich, USA), zirconium (99.5%, Strem Chemicals, USA), yttrium (Strem Chemicals, 99.9%), hafnium (99.9%, Strem Chemicals, USA). A metal to boron molar ratio of at least 1 : 20 was used to suppress the formation of lower borides ( $\text{HfB}_2$ ,  $\text{ZrB}_2$ ,  $\text{GdB}_6$ , and  $\text{YB}_6$ ) and promote the formation of dodecaboride phases ( $\text{MB}_{12}$ ). The weighed mixtures were homogenized with a vortex mixer for ~1 minute, then pressed in a hydraulic press (Carver) under ~10 tons and placed on the copper hearth in the arc-melter along with oxygen getters (zirconium metal). The chamber was then sealed and evacuated under vacuum for 20 minutes, followed by filling with argon; this was repeated at least 4 times. Before arc-melting the samples, the getters were melted in order to “absorb” any trace oxygen and finally the samples were then arc melted using  $I > 70$  amps (typically 145 amps) for  $T = 1 - 2$  min. The samples were heated until molten, flipped and re-arc'd at least 2 times to ensure homogeneity.

Subsequent ingots were then gently fractured into 2 - 4 pieces using a tool steel Plattner-style diamond crusher. For powder XRD, about half of each sample was crushed using the aforementioned tool steel Plattner-style diamond crusher into a 325 mesh ( $\leq 45 \mu\text{m}$ ) powder. PXRD was performed on a Bruker D8 Discover powder X-ray diffractometer (Bruker Corporation, Germany) utilizing a  $\text{CuK}\alpha$  X-ray beam ( $\lambda_{\text{ave}} = 1.5418 \text{ \AA}$ ,  $\lambda_{\text{K}\alpha 1} = 1.5406 \text{ \AA}$ ,  $\lambda_{\text{K}\alpha 2} = 1.5444 \text{ \AA}$ ,  $\lambda_{\text{K}\beta}$  is absorbed by a Ni filter) in the  $5 - 100^\circ 2\theta$  range with a scan speed of  $0.1055^\circ/\text{s}$ ,

time per step of 0.3 s. The phases analyzed were cross-referenced against the Joint Committee on Powder Diffraction Standards (JCPDS) database. *Maud* software was used to perform the unit cell refinements.<sup>30–34</sup>

The remaining ingots were encapsulated in an epoxy/hardener set (Allied High Tech Products Inc., USA), and then polished to an optically flat finish on a semi-automated polisher (Southbay Technology Inc., USA) using both silicon carbide abrasive disks of 120 - 1200 grit (Allied High Tech Products Inc., USA) and 30 - 1  $\mu\text{m}$  particle-size diamond films (Southbay Technology Inc., USA).

The polished samples' morphology was analyzed using an UltraDry EDS detector (Thermo Scientific, USA) and an FEI Nova 230 high-resolution scanning electron microscope (FEI Company, USA). Vickers hardness testing was performed using a MicroMet 2103 Vickers microhardness tester (Buehler Ltd., USA) with a pyramidal diamond indenter tip. 15 indents were made at applied loads of 0.49, 0.98, 1.96 N each, and a minimum of 10 indents were made at loadings of 2.94 and 4.9 N each, and were performed in random areas of the sample. A high resolution optical microscope (Zeiss Axiotech 100HD, Carl Zeiss Vision GmbH, Germany) with 500x magnification was used to measure the length of the diagonals of each indent. Vicker's hardness ( $H_v$ ) was calculated using Equation 1:

$$H_v = \frac{1854.4 F}{a^2} \quad (1)$$

where  $F$  is the loading force applied in Newtons (N),  $a$  is the average of the length of the two diagonals of each indent in micrometers ( $\mu\text{m}$ ) and  $H_v$  is Vickers hardness in gigapascals (GPa).

## RESULTS AND DISCUSSION

Powder X-ray diffraction (PXRD) and energy-dispersive X-ray spectroscopy (EDS) were used to determine the purity and phase composition of the samples. Since the primary goal of this work was to study the formation of metal dodecaborides, all samples were prepared with a metal to boron ratios of 1 to 20 in order to promote the formation of higher boride phases ( $MB_{12}$ ) and suppress the formation of lower borides ( $MB_2$  and  $MB_6$ ). Samples that were prepared with a stoichiometric amount of boron resulted in a larger proportion of lower borides in the samples.

We first prepared a solid solution between high pressure  $HfB_{12}$  and  $GdB_{12}$  by arc melting from the elements at ambient pressure. **Figure 2** shows the PXRD patterns for alloys with nominal composition of  $(Hf_{1-x}Gd_x) : 20B$  ( $x = 0.05, 0.25, 0.50, 0.75, 0.95$ ) in the  $2\Theta$  range of  $5 - 50^\circ$ . Full PXRD patterns ( $2\Theta = 5 - 80^\circ$ ) can be found in Supplemental Information **Figure S1**. **Figures 3 and 4** show the PXRD patterns for alloys with a nominal composition of  $(Zr_{1-x-z}Hf_xGd_z) : 20B$ ,  $(Y_{1-x-z}Hf_xGd_z) : 20B$ ,  $(Zr_{1-x-z}Hf_xY_z) : 20B$ ,  $(Zr_{1-x-z}Y_xGd_z) : 20B$  ( $x$  and  $z = 0.25, 0.33$  and  $0.50$ , the points were chosen in order to probe the entire ternary metal phase field) in the  $2\Theta$  range of  $5 - 50^\circ$ . Full PXRD patterns ( $2\Theta = 5 - 80^\circ$ ) can be found in Supplemental Information **Figure S2**. **Table 1** lists the values of the cubic unit cell parameters, metal concentration in the ternary dodecaboride phases and hardness values at varied applied loads of  $0.49 - 4.9$  N of force for the alloys with a nominal composition of  $(Zr_{1-x-z}Hf_xGd_z) : 20B$ ,  $(Y_{1-x-z}Hf_xGd_z) : 20B$ ,  $(Zr_{1-x-z}Hf_xY_z) : 20B$ ,  $(Zr_{1-x-z}Y_xGd_z) : 20B$  ( $x$  and  $z = 0.25, 0.33$  and  $0.50$ ). **Figure 5** shows the SEM and EDS images for alloys with a nominal composition of  $(Zr_{0.25}Hf_{0.50}Gd_{0.25}) : 20B$ ,  $(Y_{0.50}Hf_{0.25}Gd_{0.25}) : 20B$ ,  $(Zr_{0.50}Hf_{0.25}Y_{0.25}) : 20B$ ,  $(Zr_{0.25}Y_{0.25}Gd_{0.50}) : 20B$ . **Figure 6** shows the pseudo-ternary phase diagrams (boron content kept constant at 20 boron equivalents). Finally, **Figure S3** shows the optical images of the surfaces of the alloys with a nominal

composition of  $(\text{Zr}_{1-x-z}\text{Hf}_x\text{Gd}_z) : 20\text{B}$ ,  $(\text{Y}_{1-x-z}\text{Hf}_x\text{Gd}_z) : 20\text{B}$ ,  $(\text{Zr}_{1-x-z}\text{Hf}_x\text{Y}_z) : 20\text{B}$ ,  $(\text{Zr}_{1-x-z}\text{Y}_x\text{Gd}_z) : 20\text{B}$  ( $x$  and  $z = 0.25, 0.33$  and  $0.50$ ).

Both  $\text{HfB}_{12}$ <sup>25</sup> and  $\text{GdB}_{12}$ <sup>28</sup> are high pressure phases (6.5 GPa) and can be stabilized by inserting the “smaller atom into a larger host atom dodecaboride matrix”  $(\text{Y}_{1-x}\text{Hf}_x\text{B}_{12})$ <sup>19</sup> and vice versa  $(\text{Zr}_{1-x}\text{Gd}_x\text{B}_{12})$ <sup>18</sup> using the principle outlined above. Thus, a hypothetical solid solution of  $\text{Hf}_{1-x}\text{Gd}_x\text{B}_{12}$  should be stable as the larger Gd ( $1.801 \text{ \AA}$ )<sup>25</sup> will be compensated for by the smaller Hf ( $1.580 \text{ \AA}$ )<sup>25</sup>. However, when combined together in an alloy with a nominal composition of  $(\text{Hf}_{1-x}\text{Gd}_x) : 20\text{B}$  (**Figure 2**), it could be observed that no metal dodecaboride phase forms. The only phases present are diboride ( $\text{HfB}_2$ ) and  $\text{HfB}_{50}$  (at higher concentrations of hafnium) and hexaboride ( $\text{GdB}_6$ ) and  $\text{GdB}_{66}$  (at higher concentrations of gadolinium), with intermediate compositions having all of the aforementioned phases. This suggests that these two high pressure phases are unable to stabilize each other and might require a stable dodecaboride matrix in order to form at ambient pressure. Previous work had shown that  $\text{HfB}_{12}$  can be stabilized with  $\text{YB}_{12}$ , and  $\text{GdB}_{12}$  with  $\text{ZrB}_{12}$ . This is exactly what happens once Zr or Y are added to the composition, resulting in alloys with the following nominal compositions:  $(\text{Zr}_{1-x-z}\text{Hf}_x\text{Gd}_z) : 20\text{B}$ ,  $(\text{Y}_{1-x-z}\text{Hf}_x\text{Gd}_z) : 20\text{B}$  ( $x$  and  $z = 0.25$  and  $0.50$ ) (**Figure 3**).

In the case of  $(\text{Zr}_{1-x-z}\text{Hf}_x\text{Gd}_z) : 20\text{B}$  (**Figure 3a, Table 1**), a ternary metal dodecaboride ( $\text{MB}_{12}$ ) can be observed for all four compositions, with the alloys with nominal compositions of  $(\text{Zr}_{0.33}\text{Hf}_{0.33}\text{Gd}_{0.33}) : 20\text{B}$  and  $(\text{Zr}_{0.50}\text{Hf}_{0.25}\text{Gd}_{0.25}) : 20\text{B}$ , respectively, containing only the ternary dodecaboride and a boron rich phase ( $\text{Hf}_{1-x}\text{Zr}_x\text{B}_{50}$ ). The EDS analysis gives the following composition of the ternary dodecaboride:  $\text{Zr}_{0.478}\text{Hf}_{0.155}\text{Gd}_{0.367}\text{B}_{12}$  and  $\text{Zr}_{0.643}\text{Hf}_{0.104}\text{Gd}_{0.253}\text{B}_{12}$ , respectively. Since  $\text{ZrB}_{12}$  is known to stabilize  $\text{GdB}_{12}$  and the  $\text{Zr}_{1-x}\text{Gd}_x\text{B}_{12}$  solid solution exists until the concentration of gadolinium of 55 at.% Gd<sup>18</sup>, but the solubility of  $\text{HfB}_{12}$  in  $\text{ZrB}_{12}$  is very

limited<sup>19</sup>, we speculate that during the course of synthesis a meta-stable  $Zr_{1-x}Gd_xB_{12}$  matrix forms first and then stabilizes  $HfB_{12}$  in it. A similar observation can be made for the alloy with a nominal composition of  $(Y_{1-x-z}Hf_xGd_z) : 20B$  (**Figure 3b, Table 1**), where a ternary dodecaboride phase exists for three compositions. And since  $YB_{12}$  can stabilize  $HfB_{12}$  until a composition of  $Y_{0.633}Hf_{0.367}B_{12}$ , and solubility of  $GdB_{12}$  in  $YB_{12}$  is very limited, it could also be speculated that a  $Y_{1-x}Hf_xB_{12}$  matrix forms first and then stabilizes  $GdB_{12}$  in it.

For the other compositions of  $(Y_{1-x-z}Hf_xGd_z) : 20B$  (**Figure 3a, Table 1**), secondary phases (di- and hexaborides,  $Hf_{1-x}Zr_xB_2$  and  $Gd_{1-x}Y_xB_6$ ) form, resulting from the excess amount of hafnium and gadolinium over the solubility limit in the ternary dodecaboride phases. In all cases, the main boride phases are accompanied by boron-rich phases ( $Hf_{1-x}Zr_xB_{50}$  ( $R\bar{3}m$ )). For the other compositions of  $(Y_{1-x-z}Hf_xGd_z) : 20B$  (**Figure 3b, Table 1**), secondary phases (hexaborides,  $Gd_{1-x}Y_xB_6$ ) form, resulting from the excess amount of gadolinium over the solubility limit in the ternary dodecaboride phases. The main boride phases are also accompanied by boron-rich phases ( $HfB_{50}$  ( $R\bar{3}m$ ) and  $Gd_{1-x}Y_xB_{66}$  ( $Fm\bar{3}c$ )). Only in the case of the alloy with a nominal composition of  $(Y_{0.25}Hf_{0.25}Gd_{0.50}) : 20B$ , the main phase is a solid solution  $Gd_{1-x}Y_xB_6$ , resulting from a low amount of yttrium which is not enough to stabilize the ternary dodecaboride phase.

In the case of alloys with a nominal composition of  $(Zr_{1-x-z}Hf_xY_z) : 20B$  and  $(Zr_{1-x-z}Y_xGd_z) : 20B$  (**Figure 4, Table 1**), the ternary metal dodecaboride is present at all compositions. Both zirconium and yttrium form stable dodecaborides ( $ZrB_{12}$  and  $YB_{12}$ ) at ambient pressure, and thus, are completely soluble in each other, forming the  $Zr_{1-x}Y_xB_{12}$  solid solution at all compositions.<sup>17</sup> In both of these cases, the formation of ternary dodecaborides is highly favorable since for two out of three pairings of metals, the phases are either completely soluble ( $Zr_{1-x}$

${}_x\text{Y}_x\text{B}_{12}$ ) or can be stabilized at ambient pressure ( $\text{Y}_{1-x}\text{Hf}_x\text{B}_{12}$  and  $\text{Zr}_{1-x}\text{Gd}_x\text{B}_{12}$ , respectively). The secondary phases formed are diboride ( $\text{Hf}_{1-x}\text{Zr}_x\text{B}_2$ ) for an alloy with a nominal composition of  $(\text{Zr}_{0.25}\text{Hf}_{0.50}\text{Y}_{0.25}) : 20\text{B}$  and hexaboride ( $\text{Gd}_{1-x}\text{Y}_x\text{B}_6$ ) for an alloy with a nominal composition of  $(\text{Zr}_{0.25}\text{Y}_{0.25}\text{Gd}_{0.50}) : 20\text{B}$ .

**Figure 5** shows the SEM and EDS elemental maps for alloys with a nominal composition of  $(\text{Zr}_{0.25}\text{Hf}_{0.50}\text{Gd}_{0.25}) : 20\text{B}$ ,  $(\text{Y}_{0.50}\text{Hf}_{0.25}\text{Gd}_{0.25}) : 20\text{B}$ ,  $(\text{Zr}_{0.50}\text{Hf}_{0.25}\text{Y}_{0.25}) : 20\text{B}$ ,  $(\text{Zr}_{0.25}\text{Y}_{0.25}\text{Gd}_{0.50}) : 20\text{B}$ . For  $(\text{Y}_{0.50}\text{Hf}_{0.25}\text{Gd}_{0.25}) : 20\text{B}$  and  $(\text{Zr}_{0.50}\text{Hf}_{0.25}\text{Y}_{0.25}) : 20\text{B}$  a ternary metal dodecaboride phase can be observed, while for  $(\text{Zr}_{0.25}\text{Hf}_{0.50}\text{Gd}_{0.25}) : 20\text{B}$  and  $(\text{Zr}_{0.25}\text{Y}_{0.25}\text{Gd}_{0.50}) : 20\text{B}$ , lower boride phases (diborides and hexaborides, respectively) can be observed.

Based on the combined information from PXRD and EDS, one can construct limited composition pseudo-ternary (boron content is kept at a constant level of 20Boron equivalents) phase diagrams (**Figure 6**).  $(\text{Zr}_{1-x-z}\text{Hf}_x\text{Gd}_z) : 20\text{B}$ ,  $(\text{Y}_{1-x-z}\text{Hf}_x\text{Gd}_z) : 20\text{B}$ ,  $(\text{Zr}_{1-x-z}\text{Hf}_x\text{Y}_z) : 20\text{B}$ ,  $(\text{Zr}_{1-x-z}\text{Y}_x\text{Gd}_z) : 20\text{B}$ ,  $(\text{Hf}_{1-x}\text{Gd}_x) : 20\text{B}$  and  $(\text{Y}_{1-x}\text{Gd}_x) : 20\text{B}$  were analyzed in this manuscript, while data for other compositions were taken from previous publications:  $(\text{Zr}_{1-x}\text{Gd}_x) : 20\text{B}^{18}$ ,  $(\text{Zr}_{1-x}\text{Hf}_x) : 20\text{B}$ ,  $(\text{Y}_{1-x}\text{Hf}_x) : 20\text{B}^{19}$  and  $(\text{Zr}_{1-x}\text{Y}_x) : 20\text{B}^{17}$ . Although there are known phase diagrams for binary systems: B-Zr<sup>35</sup>, B-Y<sup>36</sup>, B-Gd<sup>37</sup> and B-Hf<sup>38</sup>, and some ternary systems: B-Zr-Gd, B-Hf-Gd<sup>39</sup> and B-Zr-Hf<sup>40</sup>, they do not currently exist for some other systems: B-Zr-Y, B-Y-Hf and B-Y-Gd. Therefore, although there is only a limited number of data points for the ternary boride compositions, we feel that these pseudo-ternary phase diagrams might be a helpful starting point for a complete investigation of these systems (at a constant boron level) and elucidation of more precise phase boundaries.

**Figure S3** shows the optical images of the polished surfaces for: (a)  $(\text{Zr}_{1-x-z}\text{Hf}_x\text{Gd}_z) : 20\text{B}$ ; (b)  $(\text{Y}_{1-x-z}\text{Hf}_x\text{Gd}_z) : 20\text{B}$ ; (c)  $(\text{Zr}_{1-x-z}\text{Hf}_x\text{Y}_z) : 20\text{B}$ ; (d)  $(\text{Zr}_{1-x-z}\text{Y}_x\text{Gd}_z) : 20\text{B}$ , where x and z =

0.25, 0.33 and 0.50. In all cases, the dodecaboride  $MB_{12}$  phases exhibit a color in the blue-violet range, while hexaboride  $MB_6$  phases exhibit deep blue colors, diboride phases (white streaks) are colorless, whereas other areas correspond to the boron rich (also colorless) phases:  $MB_{50}$  (for Zr and Hf) and  $MB_{66}$  (for Y and Gd). For hexa- and dodecaborides the blue color is due to the metals in +3 oxidation states (Y and Gd), while the violet color is due to the metals in +4 oxidation states (Zr and Hf).<sup>41</sup> The color range can be used as another proof of the formation of ternary dodecaboride solid solutions for most of the aforementioned alloys.

The mechanical properties of the alloys were investigated using Vickers hardness testing (**Table 1**), in hopes that the varying metal radii will result in significant solid solution hardening. In most cases of the ternary boride alloys, the hardest compositions correspond to the samples which are majority Zr or Y or at the point in the middle of the ternary metal “phase field”:  $Zr_{0.50}Hf_{0.25}Gd_{0.25} : 20B$ ,  $Y_{0.50}Hf_{0.25}Gd_{0.25} : 20B$ ,  $Zr_{0.50}Y_{0.25}Gd_{0.25} : 20B$ ;  $Zr_{0.33}Hf_{0.33}Gd_{0.33} : 20B$ ,  $Y_{0.33}Hf_{0.33}Gd_{0.33} : 20B$ ,  $Zr_{0.33}Hf_{0.33}Y_{0.33} : 20B$ ,  $Zr_{0.33}Y_{0.33}Gd_{0.33} : 20B$ . In all of these cases, the phases are harder than their “pure parent” phases. The hardest compound is  $Zr_{0.50}Y_{0.25}Gd_{0.25} : 20B$  nominal alloy composition having a hardness of  $46.9 \pm 2.4$  GPa compared to  $41.3 \pm 1.1$  and  $41.6 \pm 1.3$  GPa for alloy compositions of 1.0 Zr : 20B and 1.0 Y : 20B, respectively, at 0.49 N of applied load. It can be speculated that in all of these cases the hardness increase is due to a combination of solid-solution hardening and the differences in metal valence and atomic size.<sup>17-</sup>

19

## CONCLUSIONS

In this manuscript, we report the successful synthesis of ternary metal alloys with nominal compositions of  $(Zr_{1-x-z}Hf_xGd_z) : 20B$ ,  $(Y_{1-x-z}Hf_xGd_z) : 20B$ ,  $(Zr_{1-x-z}Hf_xY_z) : 20B$ ,  $(Zr_{1-x-z}Y_xGd_z) : 20B$  (x and z = 0.25, 0.33 and 0.5). It was discovered that for most of the compositions, a ternary

metal dodecaboride phase ( $\text{MB}_{12}$ ) forms. The hardness of all the compounds was measured, with the hardest composition being  $\text{Zr}_{0.50}\text{Y}_{0.25}\text{Gd}_{0.25}$  : 20B nominal alloy composition having a hardness of  $46.9 \pm 2.4$  GPa at 0.49 N of applied load. This value is 10% higher than its two parents 1.0 Zr : 20B and 1.0 Y : 20B. Using the data from this manuscript and previous research, pseudo-ternary phase diagrams (with a constant boron content) have been created. Although, there is a limited amount of data points for the ternary boride compositions, these pseudo-ternary phase diagrams might be a helpful starting point for a complete investigation of these systems (at a constant boron level) and elucidation of more precise phase boundaries.

#### SUPPORTING INFORMATION AVAILABLE

Full PXRD patterns for  $(\text{Zr}_{1-x-z}\text{Hf}_x\text{Gd}_z)$  : 20B,  $(\text{Y}_{1-x-z}\text{Hf}_x\text{Gd}_z)$  : 20B,  $(\text{Zr}_{1-x-z}\text{Hf}_x\text{Y}_z)$  : 20B,  $(\text{Zr}_{1-x-z}\text{Y}_x\text{Gd}_z)$  : 20B ( $x$  and  $z = 0.25, 0.33$  and  $0.5$ ),  $\text{Hf}_{1-x}\text{Gd}_x$  : 20B, ( $x = 0.05, 0.25, 0.50, 0.75$  and  $0.95$ ), and  $\text{Y}_{1-z}\text{Gd}_z$  : 20B ( $z = 0.05, 0.25, 0.50, 0.70, 0.75$  and  $0.95$ )

#### CONFLICTS OF INTEREST

There are no conflicts to declare.

#### ACKNOWLEDGEMENTS

We thank the National Science Foundation Division of Materials Research, Grant DMR-1506860 (R.B.K.) for financial support.

## REFERENCES

- 1 G. V. Samsonov, L. Y. Markovskii, A. F. Zhigach and M. G. Valyashko, *Boron, Its Compounds and Alloys [in Russian]*, House of the Academy of the Sciences Ukrainian SSR, Kiev, 1960.
- 2 G. V. Samsonov, T. I. Serebriakova and V. A. Neronov, *Borides [in Russian]*, Atomizdat, Moscow, 1975.
- 3 J. P. Scheifers, Y. Zhang and B. P. T. Fokwa, Boron: Enabling Exciting Metal-Rich Structures and Magnetic Properties, *Acc. Chem. Res.*, 2017, **50**, 2317–2325.
- 4 K. H. J. Buschow, in *Boron and Refractory Borides*, ed. V. I. Matkovich, Springer Berlin Heidelberg, Berlin, 1977, pp. 494–515.
- 5 J. Huang, Y. Yan, L. Ouyang, H. Wang, J. Liu and M. Zhu, Increased air stability and decreased dehydrogenation temperature of LiBH<sub>4</sub> via modification within poly(methylmethacrylate), *Dalt. Trans.*, 2014, **43**, 410–413.
- 6 J. Huang, Y. Yan, A. Remhof, Y. Zhang, D. Rentsch, Y. S. Au, P. E. de Jongh, F. Cuevas, L. Ouyang, M. Zhu and A. Züttel, A novel method for the synthesis of solvent-free Mg(B<sub>3</sub>H<sub>8</sub>)<sub>2</sub>, *Dalt. Trans.*, 2016, **45**, 3687–3690.
- 7 G. Akopov, M. T. Yeung and R. B. Kaner, Rediscovering the Crystal Chemistry of Borides, *Adv. Mater.*, 2017, 1604506.
- 8 G. V. Samsonov, *Refractory compounds of metals with nonmetals [in Russian]*, Metallurgiya, Moscow, 1964.
- 9 B. Albert and H. Hillebrecht, Boron: Elementary challenge for experimenters and theoreticians, *Angew. Chemie - Int. Ed.*, 2009, **48**, 8640–8668.

- 10 B. P. T. Fokwa, Borides: Solid-State Chemistry, *Encycl. Inorg. Bioinorg. Chem.*, 2014, 1–14.
- 11 T. Lundström, in *Encyclopedia of Inorganic Chemistry*, 2006, pp. 481–494.
- 12 L. E. Tergenius, Refinement of the crystal structure of orthorhombic Mn<sub>2</sub>B (formerly denoted Mn<sub>4</sub>B), *J. Less-Common Met.*, 1981, **82**, 335–340.
- 13 L. G. Bodrova, M. S. Koval'chenko and T. I. Serebryakova, Preparation of tungsten tetraboride, *Sov. Powder Metall. Met. Ceram.*, 1974, **13**, 1–3.
- 14 G. Akopov, I. Roh, Z. C. Sobell, M. T. Yeung, L. Pangilinan, C. L. Turner and R. B. Kaner, Effects of Variable Boron Concentration on the Properties of Superhard Tungsten Tetraboride, *J. Am. Chem. Soc.*, 2017, **139**, 17120–17127.
- 15 G. Akopov, M. T. Yeung, C. L. Turner, R. Mohammadi and R. B. Kaner, Extrinsic hardening of superhard tungsten tetraboride alloys with group 4 transition metals, *J. Am. Chem. Soc.*, 2016, **138**, 5714–5721.
- 16 S. La Placa, I. Binder and B. Post, Binary dodecaborides, *J. Inorg. Nucl. Chem.*, 1961, **18**, 113–117.
- 17 G. Akopov, M. T. Yeung, Z. C. Sobell, C. L. Turner and R. B. Kaner, Superhard Mixed Metal Dodecaborides, *Chem. Mater.*, 2016, **28**, 6605–6612.
- 18 G. Akopov, Z. C. C. Sobell, M. T. T. Yeung and R. B. B. Kaner, Stabilization of LnB<sub>12</sub> (Ln = Gd, Sm, Nd, and Pr) in Zr<sub>1-x</sub>Ln<sub>x</sub>B<sub>12</sub> under Ambient Pressure, *Inorg. Chem.*, 2016, **55**, 12419–12426.
- 19 G. Akopov, M. T. Yeung, C. L. Turner, R. L. Li and R. B. Kaner, Stabilization of HfB<sub>12</sub> in Y<sub>1-x</sub>Hf<sub>x</sub>B<sub>12</sub> under Ambient Pressure, *Inorg. Chem.*, 2016, **55**, 5051–5055.
- 20 S. M. Richards and J. S. Kaspar, The crystal structure of YB<sub>66</sub>, *Acta Crystallogr. Sect. B*

- Struct. Crystallogr. Cryst. Chem.*, 1969, **25**, 237–251.
- 21 A. J. Crespo, L. E. Tergenius and T. Lundstrom, The solid solution of 4d, 5d and some p elements in beta-rhombohedral boron, *J. Less-Common Met.*, 1981, **77**, 147–150.
- 22 M. T. Yeung, R. Mohammadi and R. B. Kaner, Ultraincompressible, Superhard Materials, *Annu. Rev. Mater. Res.*, 2016, **46**, 465–485.
- 23 S. T. Renosto, L. E. Corrêa, M. S. da Luz, P. F. S. Rosa, Z. Fisk, J. Albino-Aguiar and A. J. S. Machado, Superconductivity in the Th<sub>0.93</sub>Zr<sub>0.07</sub>B<sub>12</sub> compound with UB<sub>12</sub> prototype structure, *Phys. Lett. A*, 2015, **379**, 2498–2501.
- 24 V. V. Odintsov, Hardness of metal dodecaborides of UB<sub>12</sub> structure type [in Russian], *Inorg. Chem. USSR*, 1974, **10**, 366–367.
- 25 J. F. Cannon and P. B. Farnsworth, High pressure syntheses of ThB<sub>12</sub> and HfB<sub>12</sub>, *J. Less-Common Met.*, 1983, **92**, 359–368.
- 26 J. Donohue, *The Structure of the Elements*, Wiley-Interscience, New York, 1974.
- 27 W. B. Pearson, *The Crystal Chemistry and Physics of Metals and Alloys*, Wiley-Interscience, New York, 1972.
- 28 J. F. Cannon, D. M. Cannon and H. Tracy Hall, High pressure syntheses of SmB<sub>2</sub> and GdB<sub>12</sub>, *J. Less-Common Met.*, 1977, **56**, 83–90.
- 29 G. Akopov, M. T. Yeung, C. L. Turner, R. L. Li and R. B. Kaner, Stabilization of HfB<sub>12</sub> in Y<sub>1-x</sub>Hf<sub>x</sub>B<sub>12</sub> under Ambient Pressure, *Inorg. Chem.*, 2016, **55**, 5051–5055.
- 30 L. Lutterotti, D. Chateigner, S. Ferrari and J. Ricote, Texture, residual stress and structural analysis of thin films using a combined X-ray analysis, *Thin Solid Films*, 2004, **450**, 34–41.
- 31 L. Lutterotti, Maud Rev. 2.55, *Maud Rev. 2.55, Univ. Trento-Italy, Dep. Ind. Eng. Trento*,

- Italy.*
- 32 L. Lutterotti, Total pattern fitting for the combined size-strain-stress-texture determination in thin film diffraction, *Nucl. Instruments Methods Phys. Res. Sect. B Beam Interact. with Mater. Atoms*, 2010, **268**, 334–340.
  - 33 L. Lutterotti, S. Matthies, H. R. Wenk, A. S. Schultz and J. W. Richardson, Combined texture and structure analysis of deformed limestone from time-of-flight neutron diffraction spectra, *J. Appl. Phys.*, 1997, **81**, 594–600.
  - 34 L. Lutterotti, M. Bortolotti, G. Ischia, I. Lonardelli and H. R. Wenk, Rietveld texture analysis from diffraction images, *Zeitschrift fur Krist. Suppl.*, 2007, **1**, 125–130.
  - 35 K. I. Portnoi, V. M. Romashev and L. N. Burobina, Constitution Diagram of the System Zirconium-Boron, *Powder Metall. Met. Ceram.*, 1970, **7**, 68–71.
  - 36 P. K. Liao and K. E. Spear, The B-Y (boron-yttrium) system, *J. Phase Equilibria*, 1995, **16**, 521–524.
  - 37 P. K. Liao, K. E. Spear and M. E. Schlesinger, The B-Gd ( Boron-Gadolinium ) System, 1996, **17**, 330–334.
  - 38 K. I. Portnoi, V. M. Romashov, I. V. Romanovich, Y. V. Levinskii and S. A. Prokof'ev, Phase diagram of the system Hf-B, *Inorg. Mater.*, 1971, **7**, 1769–1772.
  - 39 N. F. Chaban and Y. B. Kuz'ma, {Ti, Zr, Hf}-Gd-B Systems, *Sov. Powder Metall. Met. Ceram.*, 1978, **17**, 592–593.
  - 40 E. Rudy, Zr-Hf-B System, *Comp. Phase Diagr. Data, Ternary Phase Equilib. TM-B-C-Si, AFML-Tr-65-2, Part V*, 1969, 562–581.
  - 41 R. W. Mar and N. D. Stout, High Temperature Enthalpies of Binary Dodecaborides, *J. Chem. Phys.*, 1972, **57**, 5342–5349.

- 42 L. Vegard, Die Konstitution der Mischkristalle und die Raumfullung der Atome, *Zeitschrift fur Phys.*, 1921, **5**, 17–26.
- 43 A. Leithe-Jasper, A. Sato and T. Tanaka, Refinement of the crystal structure of zirconium dodecaboride, ZrB<sub>12</sub>, at 140 K and 293 K, *Zeitschrift fur Krist. - New Cryst. Struct.*, 2002, **217**, 319–320.
- 44 B. Callmer, A Single-Crystal Diffractometry Boron Investigation of Scandium in beta-rhombohedral boron, *J. Solid State Chem.*, 1978, **23**, 391–398.
- 45 G. A. Slack, C. I. Hejna, M. Garbaskas and J. S. Kasper, X-ray study of transition-metal dopants in beta-boron, *J. Solid State Chem.*, 1988, **76**, 64–86.

**Table 1.** Unit Cell Data and Compositions for  $(\text{Zr}_{1-x-z}\text{Hf}_x\text{Gd}_z) : 20\text{B}$ ,  $(\text{Y}_{1-x-z}\text{Hf}_x\text{Gd}_z) : 20\text{B}$ ,  $(\text{Zr}_{1-x-z}\text{Hf}_x\text{Y}_z) : 20\text{B}$ ,  $(\text{Zr}_{1-x-z}\text{Y}_x\text{Gd}_z) : 20\text{B}$ 

Nominal Composition	MB <sub>12</sub> Cubic Cell (Å)			Metal Concentration (EDS) <sup>c</sup> (at. % metal)			Vickers Hardness (GPa) <sup>d</sup>									
	$a_{\text{nom}}$ <sup>a</sup>	$a_{\text{XRD}}$ <sup>b</sup>	$a_{\text{EDS}}$ <sup>a</sup>	M <sub>1</sub>	M <sub>2</sub>	M <sub>3</sub>	0.49 N		0.98 N		1.96 N		2.98 N		4.9 N	
Zr <sub>0.33</sub> Hf <sub>0.33</sub> Gd <sub>0.33</sub> : 20B	7.362	7.458(2)	7.446	47.78	15.54	36.68	42.1	2.3	35.4	1.1	33.3	0.7	32.0	0.9	29.4	1.0
Zr <sub>0.50</sub> Hf <sub>0.25</sub> Gd <sub>0.25</sub> : 20B	7.429	7.448(3)	7.434	64.29	10.38	25.33	43.7	1.8	36.9	1.2	34.3	1.6	31.8	0.9	29.4	1.2
Zr <sub>0.25</sub> Hf <sub>0.50</sub> Gd <sub>0.25</sub> : 20B	7.422	7.454(2)	7.448	49.94	12.35	37.71	41.9	1.6	33.9	1.2	31.5	1.5	30.2	0.8	28.1	0.7
Zr <sub>0.25</sub> Hf <sub>0.25</sub> Gd <sub>0.50</sub> : 20B	7.458	7.453(5)	7.445	41.08	21.17	37.74	42.4	3.5	36.5	1.4	33.7	1.9	32.3	1.6	30.2	1.4
Y <sub>0.33</sub> Hf <sub>0.33</sub> Gd <sub>0.33</sub> : 20B	7.394	7.484(4)	7.488	57.04	16.79	26.17	44.8	2.0	34.6	1.3	32.0	1.8	30.9	1.3	28.5	1.8
Y <sub>0.50</sub> Hf <sub>0.25</sub> Gd <sub>0.25</sub> : 20B	7.478	7.488(3)	7.480	64.85	21.73	13.42	43.2	2.0	37.4	1.5	33.8	1.5	31.9	1.7	30.8	0.7
Y <sub>0.25</sub> Hf <sub>0.50</sub> Gd <sub>0.25</sub> : 20B	7.446	7.472(3)	7.474	44.62	28.13	27.25	43.2	2.8	35.9	2.1	33.3	2.1	31.8	1.9	28.6	1.2
Y <sub>0.25</sub> Hf <sub>0.25</sub> Gd <sub>0.50</sub> : 20B	7.483	N/A	N/A	N/A	N/A	N/A	37.6	4.0	30.9	1.8	27.1	1.0	25.7	1.8	25.4	1.8
Zr <sub>0.33</sub> Hf <sub>0.33</sub> Y <sub>0.33</sub> : 20B	7.357	7.442(1)	7.445	43.88	14.61	41.51	45.2	2.6	35.0	1.6	32.3	1.3	30.9	1.3	29.9	0.5
Zr <sub>0.50</sub> Hf <sub>0.25</sub> Y <sub>0.25</sub> : 20B	7.427	7.460(1)	7.437	59.35	10.01	30.63	42.0	2.8	36.4	2.1	31.6	1.4	29.6	1.6	29.5	0.8
Zr <sub>0.25</sub> Hf <sub>0.50</sub> Y <sub>0.25</sub> : 20B	7.418	7.435(3)	7.460	32.19	11.48	56.33	44.2	2.8	35.5	1.7	33.0	1.7	31.9	1.6	29.3	1.3
Zr <sub>0.25</sub> Hf <sub>0.25</sub> Y <sub>0.50</sub> : 20B	7.450	7.436(4)	7.450	32.52	19.35	48.12	41.9	2.9	33.8	1.4	30.4	1.3	29.9	1.2	29.2	1.0
Zr <sub>0.33</sub> Y <sub>0.33</sub> Gd <sub>0.33</sub> : 20B	7.406	7.480(6)	7.472	40.83	35.21	23.97	42.1	2.6	33.4	1.8	31.9	1.2	30.2	1.0	27.5	0.4
Zr <sub>0.50</sub> Y <sub>0.25</sub> Gd <sub>0.25</sub> : 20B	7.463	7.460(2)	7.453	59.48	24.26	16.27	46.9	2.4	35.1	1.0	32.2	1.7	30.6	1.3	28.7	1.3
Zr <sub>0.25</sub> Y <sub>0.50</sub> Gd <sub>0.25</sub> : 20B	7.487	7.486(3)	7.477	33.72	50.18	16.09	41.1	1.9	33.5	1.7	30.8	1.1	29.3	0.8	28.0	0.7
Zr <sub>0.25</sub> Y <sub>0.25</sub> Gd <sub>0.50</sub> : 20B	7.491	7.480(3)	7.465	49.16	20.17	30.67	42.1	2.5	36.0	1.9	32.9	1.6	31.1	1.5	29.3	1.5
1.0 Zr : 20B	7.408	7.412(2)	-	-	-	-	41.3	1.1	34.9	0.5	33.6	0.7	31.3	0.6	29.6	0.7
1.0 Y : 20B	7.500	7.505(4)	-	-	-	-	41.6	1.3	34.4	1.3	32.7	1.1	30.5	0.8	28.5	0.7
Y <sub>0.25</sub> Hf <sub>0.75</sub> : 20B <sup>e</sup>	7.409	7.458(3)	7.463	66.99	33.01	-	44.1	1.7	36.5	1.2	34.6	0.8	31.9	0.7	30.8	0.7
Zr <sub>0.50</sub> Gd <sub>0.50</sub> : 20B <sup>e</sup>	7.468	7.464(2)	7.469	49.17	50.83	-	42.1	1.9	34.7	1.1	32.6	0.7	31.9	0.6	29.1	0.5

<sup>a</sup>calculated from nominal and EDS metal compositions using Vegard's Law<sup>42</sup>; <sup>b</sup>from Maud<sup>30-34</sup>, errors are given in brackets ( $a(\text{ZrB}_{12}) = 7.408 \text{ \AA}$ ,  $a(\text{YB}_{12}) = 7.500 \text{ \AA}$ ,  $a(\text{GdB}_{12}) = 7.524 \text{ \AA}$ ,  $a(\text{HfB}_{12}) = 7.377 \text{ \AA}$ );<sup>16,25,28</sup> <sup>c</sup>errors for EDS values of metal compositions are within  $\pm 2.0$  at.%, M<sub>1</sub> = Zr or Y, M<sub>2</sub> = Hf or Y, M<sub>3</sub> = Y or Gd; <sup>d</sup>errors for hardness are given next to the hardness values; <sup>e</sup>since both HfB<sub>12</sub> and GdB<sub>12</sub> are high pressure phases, these solid solutions are the closest representation of the properties of these high pressure phases.<sup>18,19</sup>

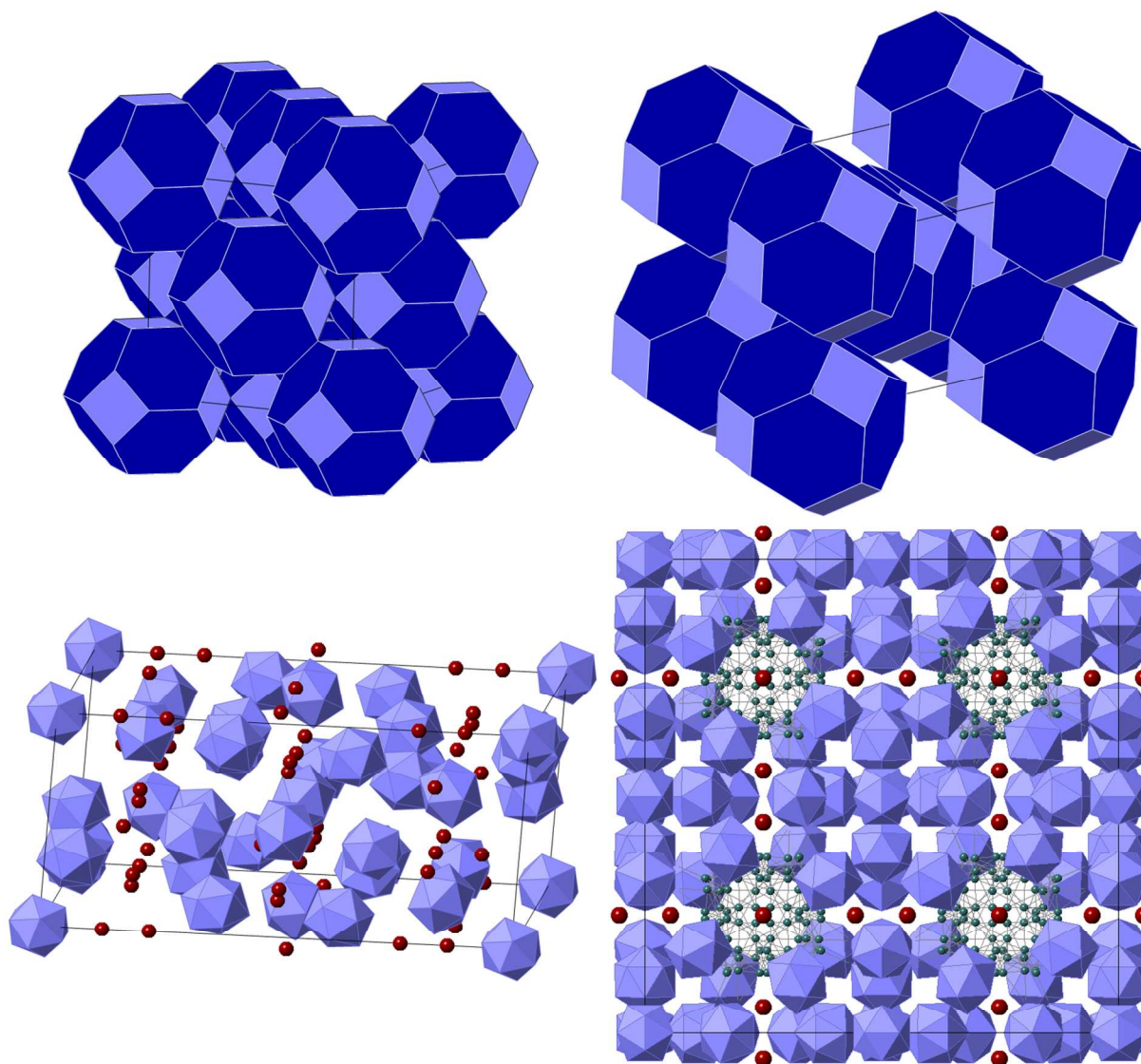


**Figure 1.** (Top left) Polyhedra model of the unit cell of a cubic- $\text{UB}_{12}$  ( $\text{ZrB}_{12}$ ,  $Fm\bar{3}m$ , ICSD 409635)<sup>43</sup> structural type metal dodecaboride; (top right) polyhedra model of the unit cell of a tetragonal- $\text{ScB}_{12}$  ( $\text{ScB}_{12}$ ,  $I4/mmm$ , ICSD 615424)<sup>44</sup> structural type metal dodecaboride; (bottom left) polyhedra model of the unit cell of a rhombohedral- $\text{MB}_{50}$  ( $R\bar{3}m$ , ICSD 40396)<sup>45</sup> structural type (solid solution of a metal in  $\beta$ -rhombohedral boron); (bottom right) polyhedra model of the unit cell of a cubic- $\text{YB}_{66}$  ( $Fm\bar{3}c$ , ICSD 23186)<sup>20</sup> structural type metal boride. In the latter two cases boron atoms are arranged in  $\text{B}_{12}$  icosahedral units. "Reprinted (adapted) with permission from (Akopov, G., Sobell, Z.C., Yeung, M.T., and Kaner, R.B. *Inorganic Chemistry* **2016** 55 (23), 12419-12426 DOI: 10.1021/acs.inorgchem.6b02311). Copyright (2016) American Chemical Society."

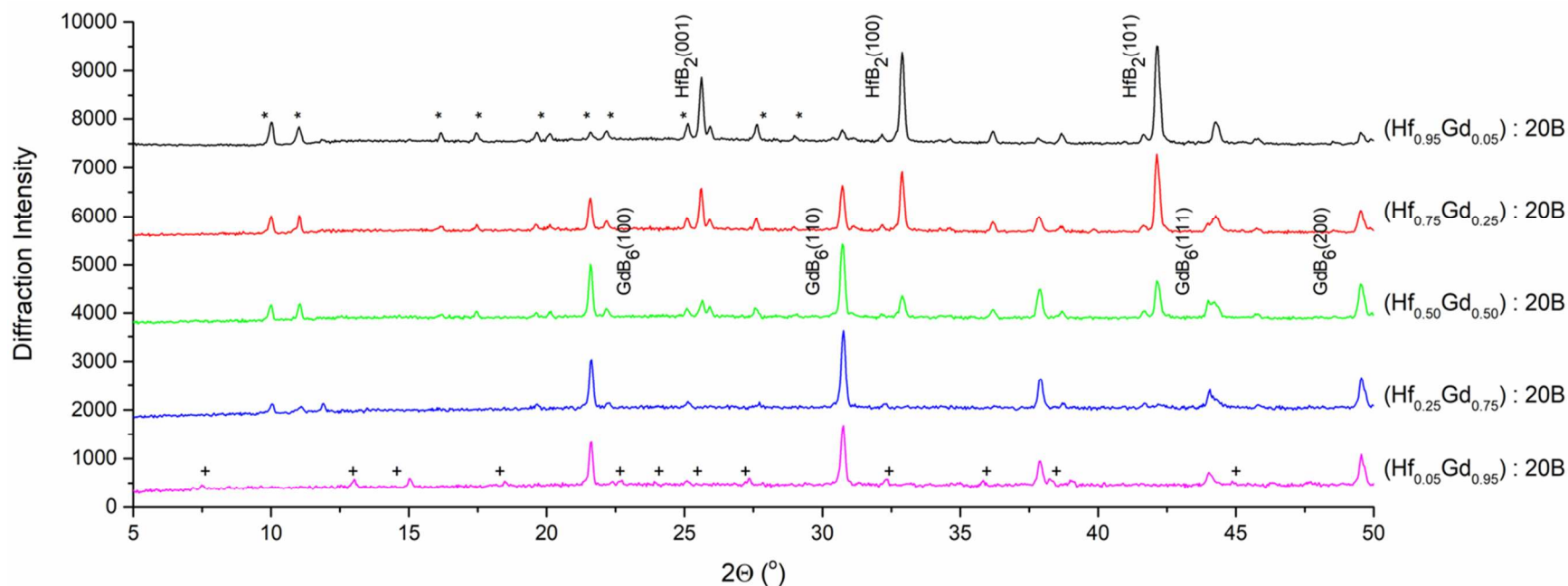
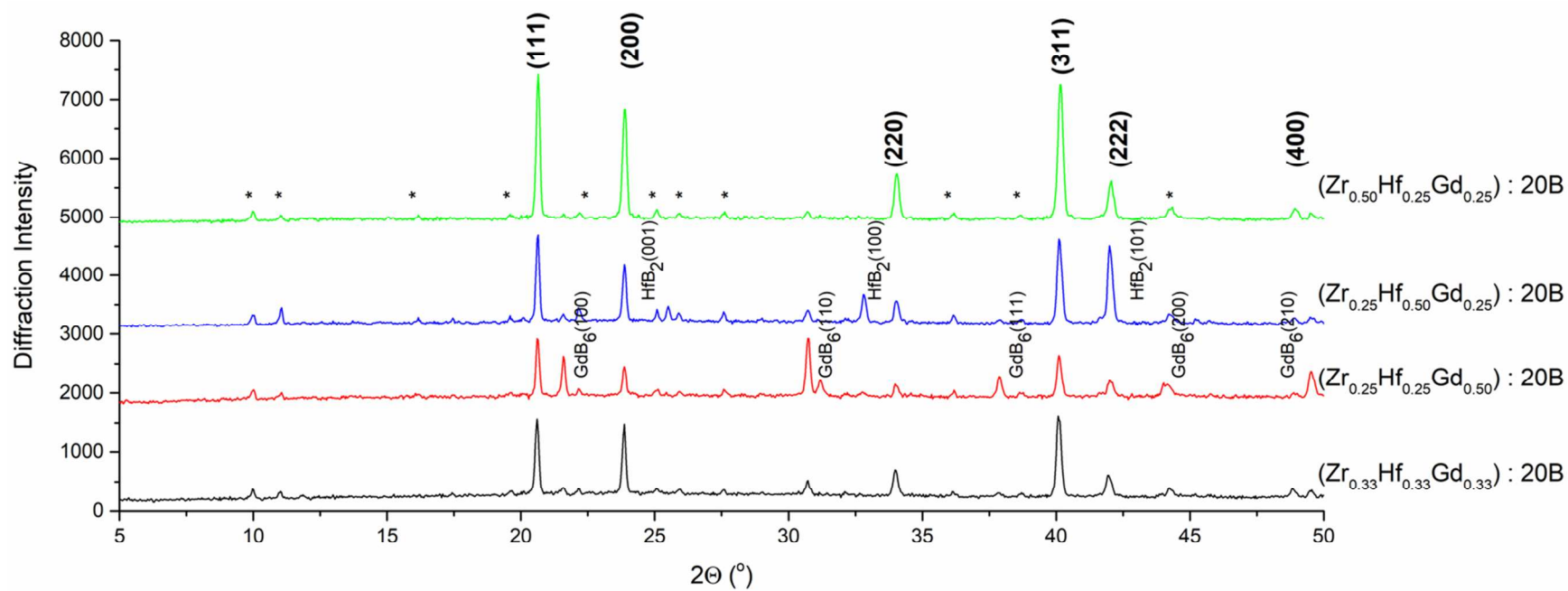
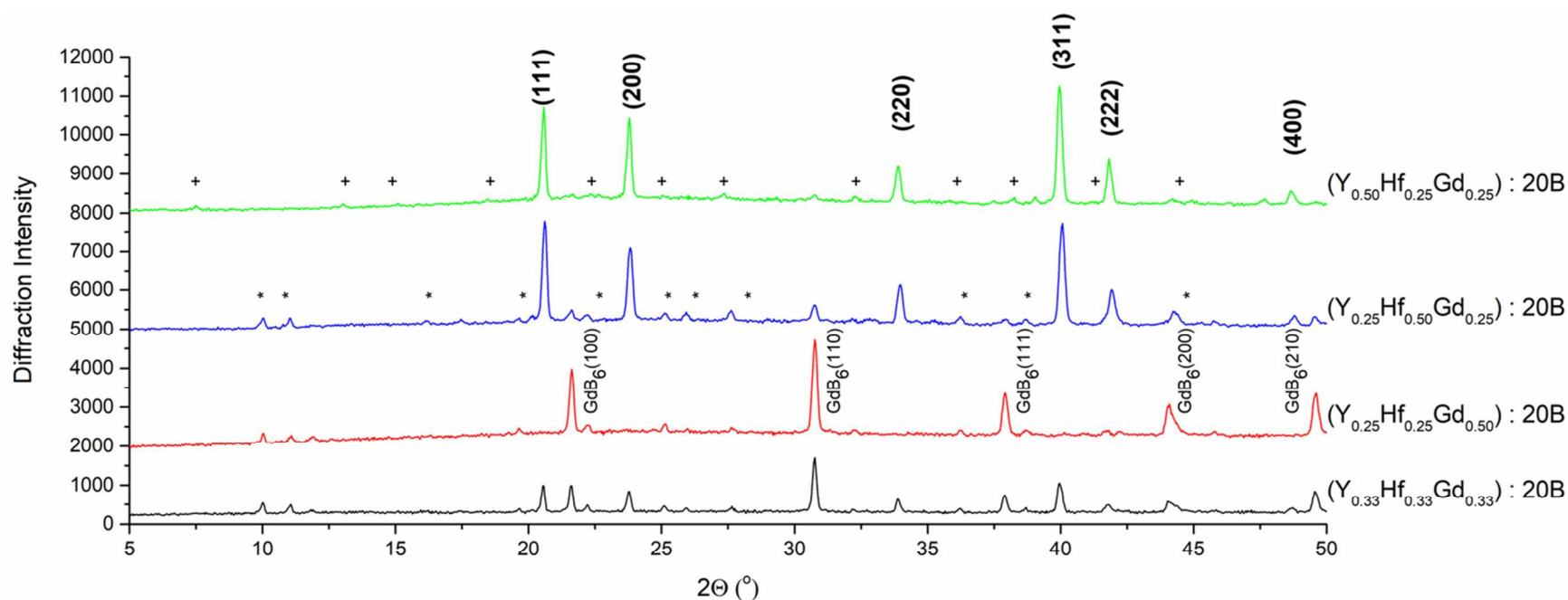


**Figure 2.** Powder XRD patterns of  $(\text{Hf}_{1-x}\text{Gd}_x) : 20\text{B}$ , where  $x = 0.05, 0.25, 0.50, 0.75$  and  $0.95$ . The dodecaboride  $\text{MB}_{12}$  phase does not form for any composition of this alloy. The diboride ( $\text{HfB}_2$ ,  $P6/mmm$ , JCPDS 03-065-3387) phase forms at higher concentrations of hafnium, while the hexaboride ( $\text{GdB}_6$ ,  $Pm\bar{3}m$ , JCPDS 03-065-1826) phase forms for higher concentrations of gadolinium. (\*) indicates the boron rich phase - solid solution of hafnium in  $\beta$ -rhombohedral boron ( $\text{HfB}_{50}$ ,  $R\bar{3}m$ , JCPDS 01-086-2400), while (+) indicates  $\text{GdB}_{66}$  ( $Fm\bar{3}c$ , JCPDS 00-024-1256). The figure shows a  $2\theta$  range from  $0 - 50^\circ$  (the full PXRD patterns are provided in the Supplemental Information section, **Figure S1**).

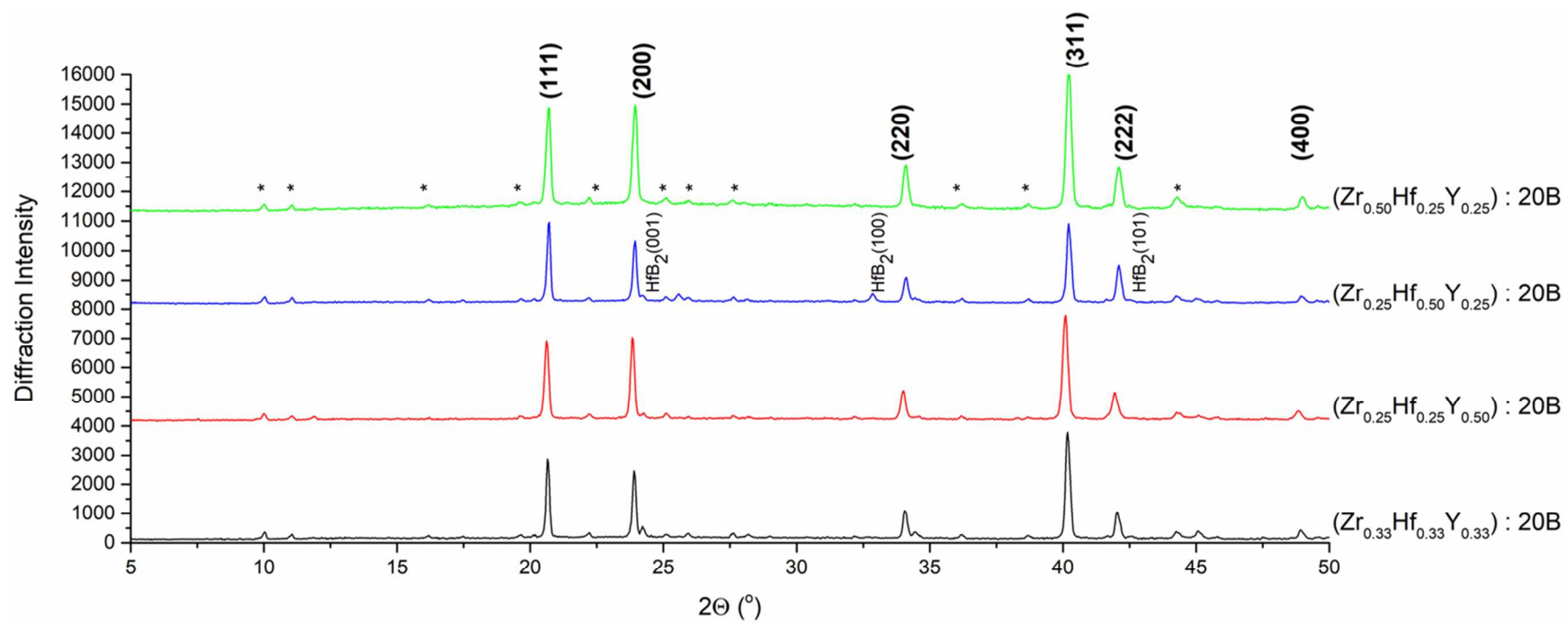


(a)

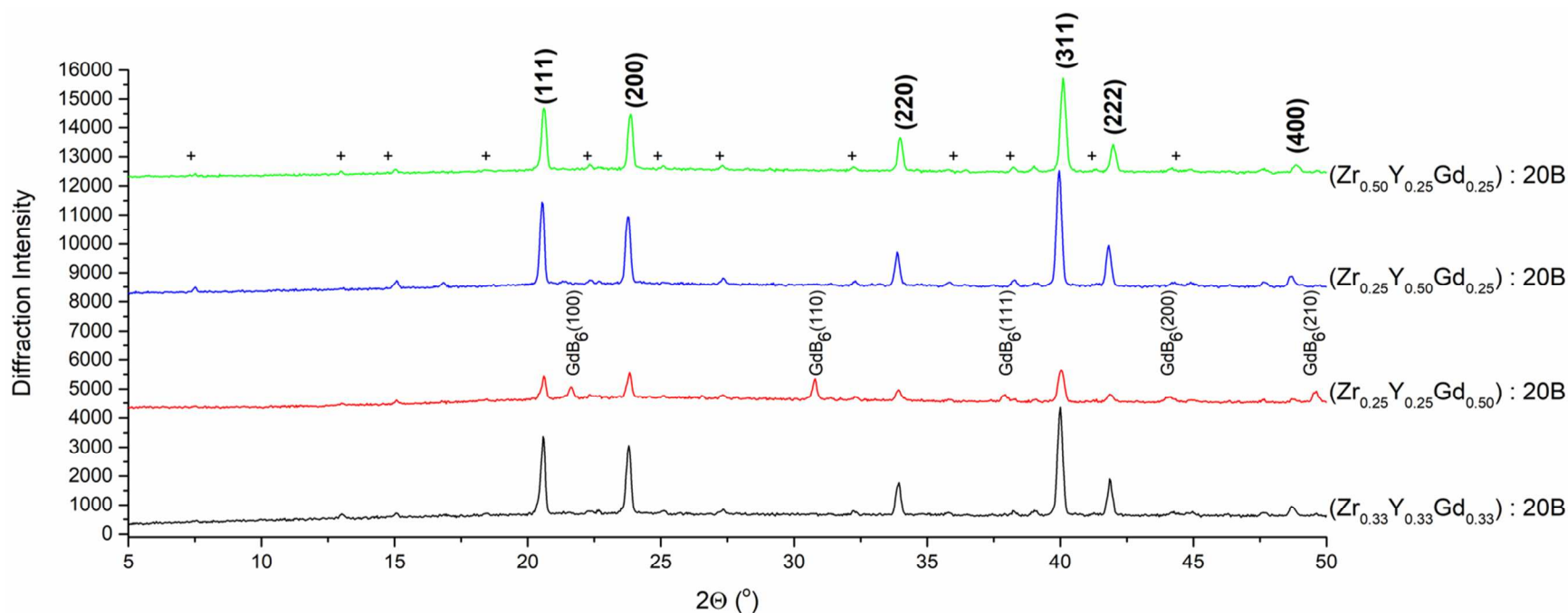


(b)

**Figure 3.** Powder XRD patterns of: (a)  $(\text{Zr}_{1-x-z}\text{Hf}_x\text{Gd}_z) : 20\text{B}$ , where  $x$  and  $z = 0.25, 0.33$  and  $0.50$ . The ternary dodecaboride  $\text{MB}_{12}$  phase can be observed for all 4 compositions, the binary diboride  $\text{MB}_2$  phase ( $\text{Hf}_{1-x}\text{Zr}_x\text{B}_2$  solid solution) can be observed for  $\text{Zr}_{0.25}\text{Hf}_{0.50}\text{Gd}_{0.25} : 20\text{B}$ , while the hexaboride  $\text{MB}_6$  phase ( $\text{GdB}_6$ ) can be observed for all phases except for  $\text{Zr}_{0.50}\text{Hf}_{0.25}\text{Gd}_{0.25} : 20\text{B}$ ; (b)  $(\text{Y}_{1-x-z}\text{Hf}_x\text{Gd}_z) : 20\text{B}$ , where  $x$  and  $z = 0.25, 0.33$  and  $0.50$ . The ternary dodecaboride  $\text{MB}_{12}$  phase can be observed for all compositions, except for  $\text{Y}_{0.25}\text{Hf}_{0.25}\text{Gd}_{0.50} : 20\text{B}$ , while the binary hexaboride  $\text{MB}_6$  phase ( $\text{Gd}_{1-x}\text{Y}_x\text{B}_6$  solid solution) can be observed for all compositions except for  $\text{Y}_{0.50}\text{Hf}_{0.25}\text{Gd}_{0.25} : 20\text{B}$ . The ternary dodecaboride  $\text{MB}_{12}$  phase can be observed for both compositions. For all cases: (\*) indicates the boron rich phase - solid solution of hafnium-zirconium in  $\beta$ -rhombohedral boron ( $\text{Hf}_{1-x}\text{Zr}_x\text{B}_{50}$ ), both  $R\bar{3}m$ , JCPDS 01-086-2400 and 03-065-2184, respectively); while (+) indicates  $\text{GdB}_{66}$  and  $\text{YB}_{66}$  or their solid solutions (both  $Fm\bar{3}c$ , JCPDS 00-024-1256 and 01-073-0759, respectively). The peaks were assigned using:  $\text{HfB}_2$ ,  $P6/mmm$ , JCPDS 03-065-3387,  $\text{GdB}_6$ ,  $Pm\bar{3}m$ , JCPDS 03-065-1826 and  $\text{ZrB}_{12}$ ,  $Fm\bar{3}m$ , JCPDS 03-065-3100. The figure shows a  $2\theta$  range from  $0 - 50^\circ$  (the full PXRD patterns are provided in the Supplemental Information section, **Figure S2**).

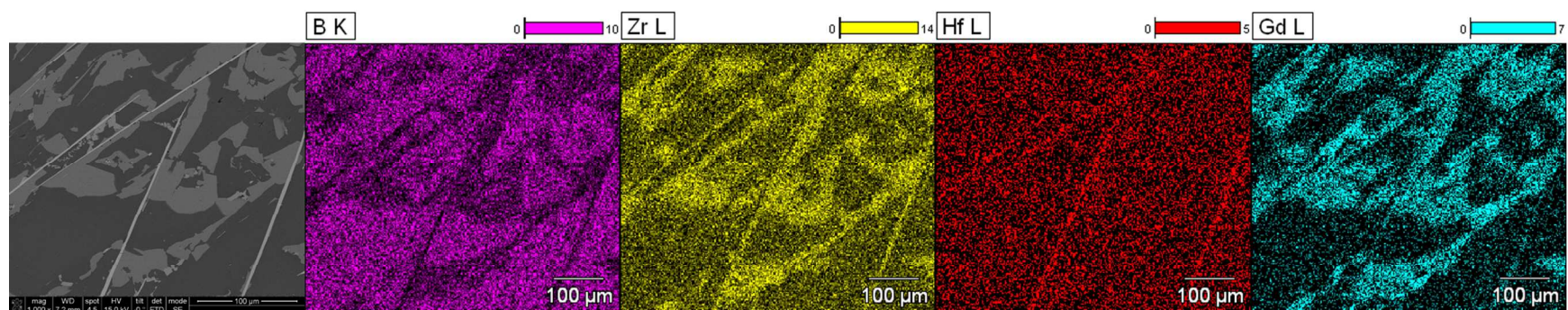


(a)

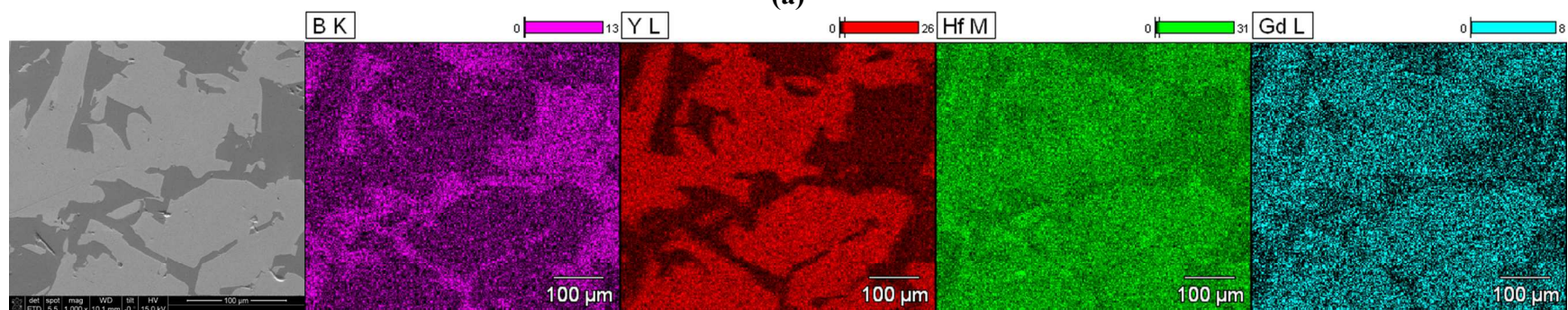


(b)

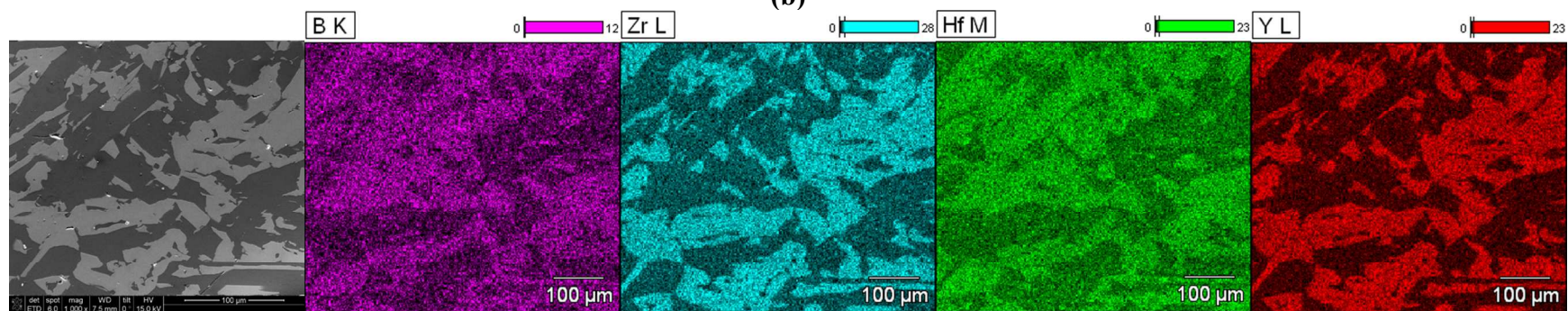
**Figure 4.** Powder XRD patterns of: (a)  $(\text{Zr}_{1-x-z}\text{Hf}_x\text{Y}_z) : 20\text{B}$ , where  $x$  and  $z = 0.25, 0.33$  and  $0.50$ . The ternary dodecaboride  $\text{MB}_{12}$  phase can be observed for all 4 compositions, the binary diboride  $\text{MB}_2$  phase ( $\text{Hf}_{1-x}\text{Zr}_xB_2$  solid solution) can be observed for  $\text{Zr}_{0.25}\text{Hf}_{0.50}\text{Y}_{0.25} : 20\text{B}$ , while the hexaboride  $\text{MB}_6$  phase ( $\text{YB}_6$ ) can be observed for all phases except for  $\text{Zr}_{0.50}\text{Hf}_{0.25}\text{Y}_{0.25} : 20\text{B}$ ; (b)  $(\text{Zr}_{1-x-z}\text{Y}_x\text{Gd}_z) : 20\text{B}$ , where  $x$  and  $z = 0.25, 0.33$  and  $0.50$ . The ternary dodecaboride  $\text{MB}_{12}$  phase can be observed for all 4 compositions, the binary hexaboride  $\text{MB}_6$  phase ( $\text{Gd}_{1-x}\text{Y}_xB_6$  solid solution) can be observed for  $\text{Zr}_{0.25}\text{Y}_{0.25}\text{Gd}_{0.50} : 20\text{B}$ . For all cases: (\*) indicates the boron rich phase - solid solution of hafnium-zirconium in  $\beta$ -rhombohedral boron ( $\text{Hf}_{1-x}\text{Zr}_xB_{50}$ ), both  $R\bar{3}m$ , JCPDS 01-086-2400 and 03-065-2184, respectively); while (+) indicates  $\text{GdB}_{66}$  and  $\text{YB}_{66}$  or their solid solutions (both  $Fm\bar{3}c$ , JCPDS 00-024-1256 and 01-073-0759, respectively). The peaks were assigned using:  $\text{HfB}_2$ ,  $P6/mmm$ , JCPDS 03-065-3387,  $\text{GdB}_6$ ,  $Pm\bar{3}m$ , JCPDS 03-065-1826 and  $\text{ZrB}_{12}$ ,  $Fm\bar{3}m$ , JCPDS 03-065-3100. The figure shows a  $2\theta$  range from  $0 - 50^\circ$  (the full PXRD patterns are provided in the Supplemental Information section, **Figure S2**).



(a)



(b)



(c)

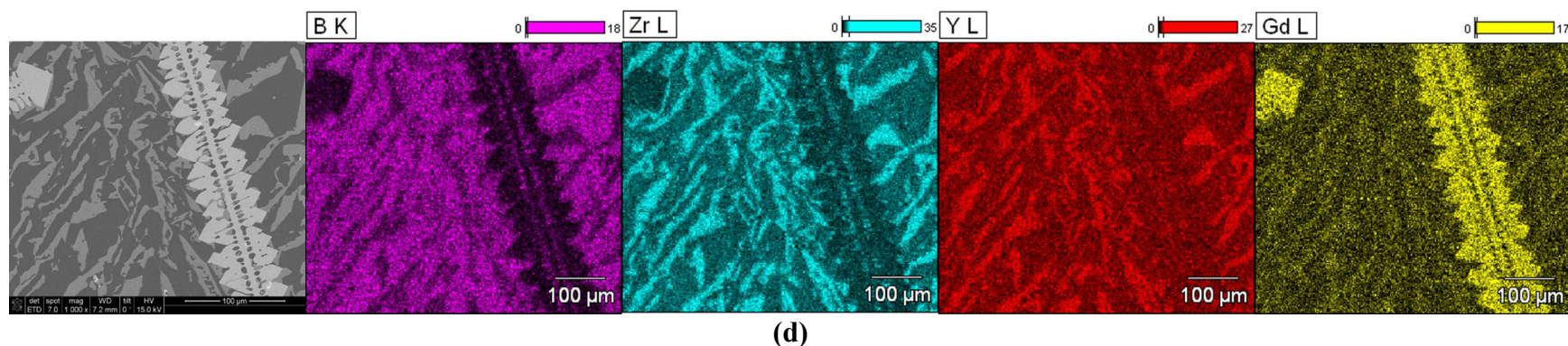
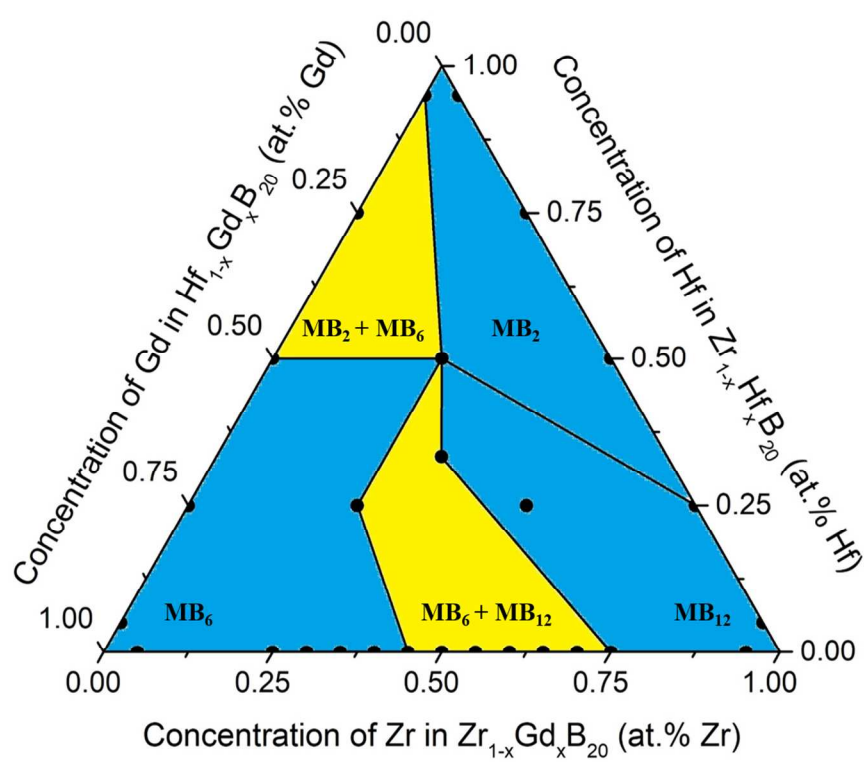
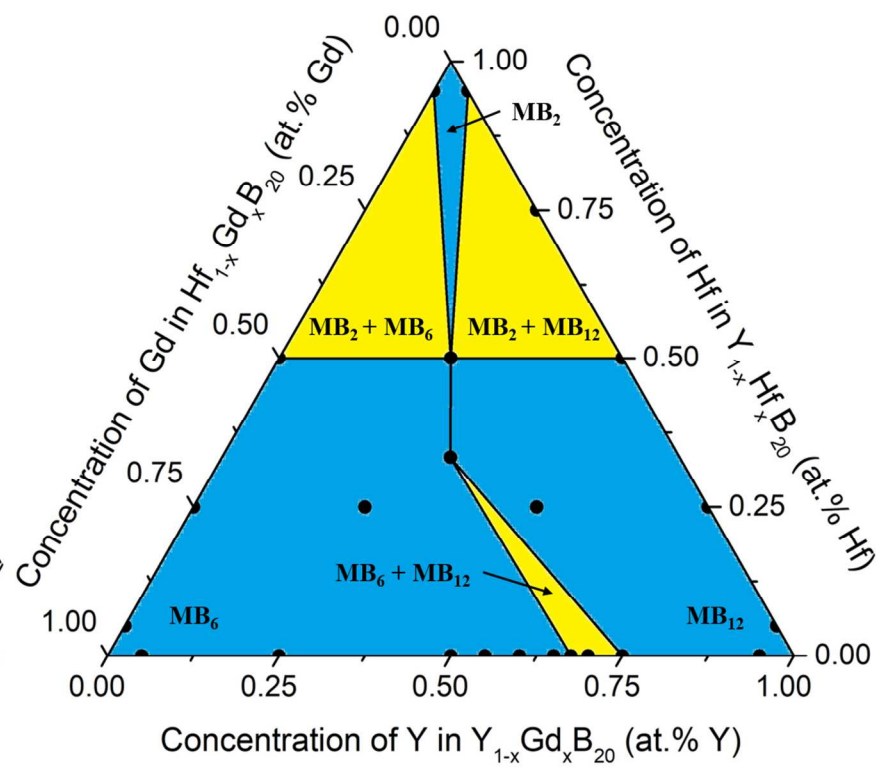


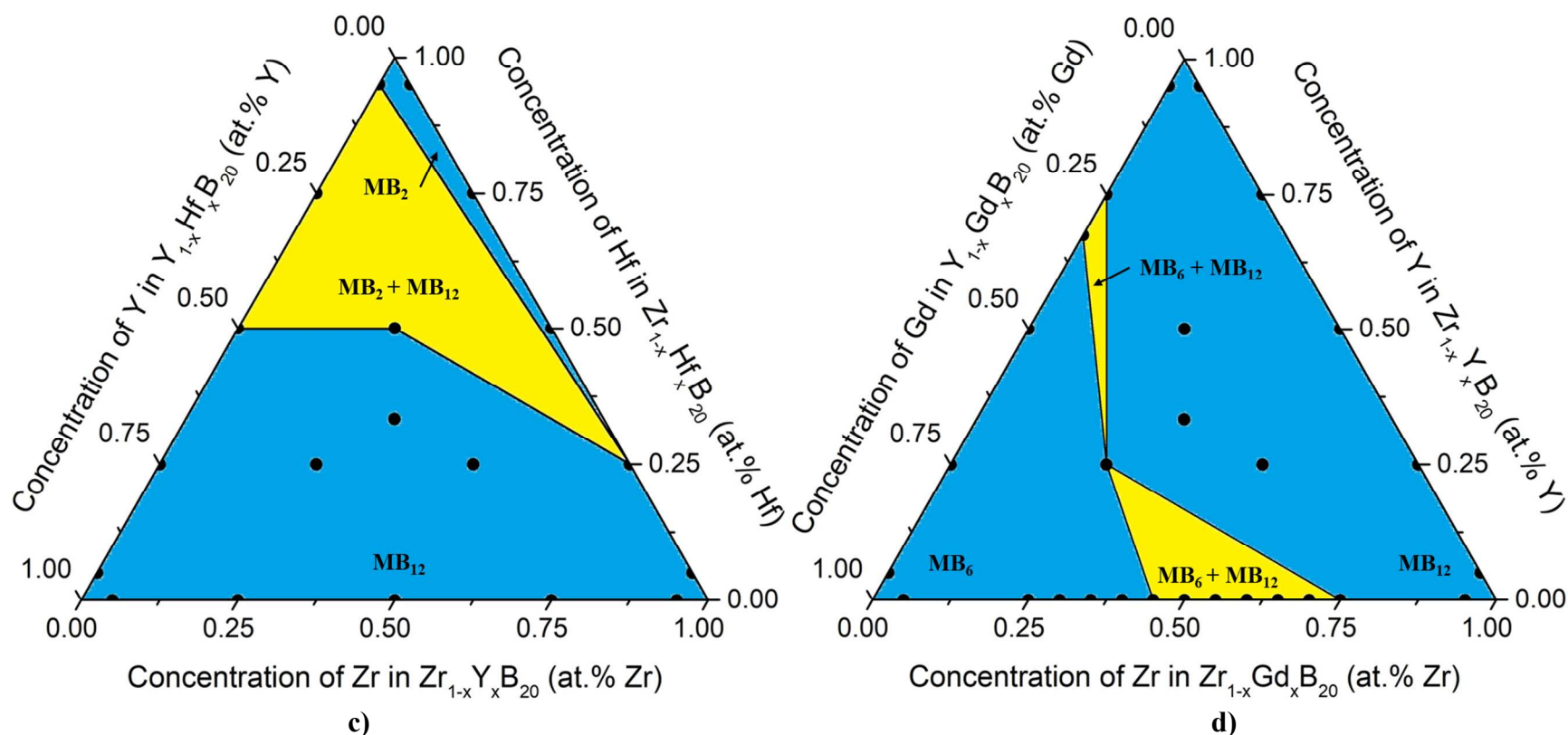
**Figure 5.** Elemental maps for boron (K line), zirconium, yttrium, gadolinium (L lines) and hafnium (M line) of: (a) the  $Zr_{0.25}Hf_{0.50}Gd_{0.25} : 20B$ , dodecaboride  $MB_{12}$  as well as  $Zr_{1-x}Hf_xB_2$  solid solution phases; (b)  $Y_{0.50}Hf_{0.25}Gd_{0.25} : 20B$ , dodecaboride  $MB_{12}$  phase; (c)  $Zr_{0.50}Hf_{0.25}Y_{0.25} : 20B$ , dodecaboride  $MB_{12}$  phase; (d)  $Zr_{0.25}Y_{0.50}Gd_{0.25} : 20B$ , dodecaboride  $MB_{12}$  as well as hexaboride  $GdB_6$  phases. The thick horizontal bars represent the intensity as a color legend. The SEM images were taken at a magnification of 1000x, while the EDS images at 500x, the scale bars are 100  $\mu m$  in all cases.



a)



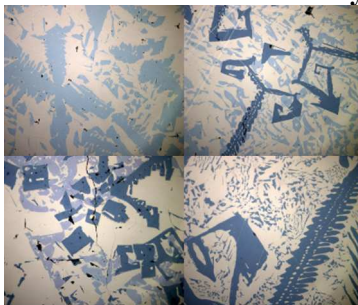
b)



**Figure 5.** Pseudo-ternary phase diagrams (limited compositions, metal to boron ratio is kept constant at 1 : 20) for: (a)  $(Zr_{1-x-z}Hf_xGd_z) : 20B$ ; (b)  $(Y_{1-x-z}Hf_xGd_z) : 20B$ ; (c)  $(Zr_{1-x-z}Hf_xY_z) : 20B$ ; (d)  $(Zr_{1-x-z}Y_xGd_z) : 20B$ . In all cases  $x$  and  $z = 0.25, 0.33$  and  $0.50$ ; black dots correspond to the analyzed compositions; the blue regions correspond to compositions with single boride phases, while yellow regions to compositions with two distinct boride phases.  $MB_{12}$  corresponds to ternary dodecaborides of Zr, Y, Hf and Gd;  $MB_2$  to binary diborides ( $Hf_{1-x}Zr_xB_2$ ); and  $MB_6$  to binary hexaborides ( $Gd_{1-x}Y_xB_6$ ). Due to the excess of boron in the samples, in all cases the main boride phases are accompanied by boron rich phases and their solid solutions:  $MB_{50}$  (for Zr and Hf) and  $MB_{66}$  (for Y and Gd).  $(Zr_{1-x-z}Hf_xGd_z) : 20B$ ,  $(Y_{1-x-z}Hf_xGd_z) : 20B$ ,  $(Zr_{1-x-z}Hf_xY_z) : 20B$ ,  $(Zr_{1-x-z}Y_xGd_z) : 20B$ ,  $(Hf_{1-x}Gd_x) : 20B$  and  $(Y_{1-x}Gd_x) : 20B$  were analyzed in this manuscript, while data for other compositions were taken from previous publications:  $(Zr_{1-x}Gd_x) : 20B$ <sup>18</sup>,  $(Zr_{1-x}Hf_x) : 20B$ ,  $(Y_{1-x}Hf_x) : 20B$ <sup>19</sup> and  $(Zr_{1-x}Y_x) : 20B$ <sup>17</sup>.

**For Table of Content Only**

Optical images of the surface patterns formed by hexaboride ( $\text{MB}_6$ ) and dodecaboride ( $\text{MB}_{12}$ ) phases.

**For Table of Content Only**

Optical images of the surface patterns formed by hexaboride ( $\text{MB}_6$ ) and dodecaboride ( $\text{MB}_{12}$ ) phases.